Stable discrete soliton molecules in two-dimensional waveguide arrays

P. S. Vinayagam, Amaria Javed, and U. Al Khawaja*
Department of Physics, United Arab Emirates University, P.O. Box 15551, Al-Ain, United Arab Emirates

(Received 11 October 2018; published 26 December 2018)

We consider a bound state of two discrete solitons in a two-dimensional waveguide array. Using numerical and variational calculations, we investigate the effect of binding on the mobility of the two solitons, which we found to be marginal. Considering anisotropic waveguides, where coupling in one direction is stronger than in the other, we show that mobility is enhanced considerably along the weaker-coupling direction. We show also that a stable bound state of two solitons exists in such a setup where each one of the two solitons is located at a different waveguide. The stability of the resulting soliton molecule is provided by the Peierls-Nabarro potential and the mobility of the individual solitons is facilitated by the anisotropy. Considering a combination of two out-of-phase solitons, we find that they form a metastable state of a single soliton that suddenly splits into two solitons propagating away from each other.

DOI: 10.1103/PhysRevA.98.063839

I. INTRODUCTION

Discrete solitons were shown to exist in arrays of coupled waveguides [1,2] exhibiting unique behavior in contrast with their continuum counterparts. This was revealed through a number of phenomena [3–11]. Prominent among these is the dissipative flow due to the presence of the Peierls-Nabarro (PN) effective potential [7–10]. Due to its crucial effect on the soliton stability and dynamics, the height and profile of the PN potential has been extensively investigated by many authors [8,12]. Interest in discrete solitons was then boosted by their application in the all-optical operations [13].

The experimental observation of discrete solitons in two-dimensional (2D) optically induced nonlinear photonic lattices [14] stimulated further interest due to the additional advantages brought by the dimensionality [15–17]. Three fundamental types of 2D stationary solitons were found, namely, the site-centered, bond-centered, and hybrid solitons [18]. Recently, we have shown that with anisotropic waveguide arrays the hybrid soliton splits into two types, namely, the hybrid-X and hybrid-Y solitons [19]. We have also shown that anisotropy greatly enhances the mobility of discrete solitons. In general, two-dimensional discrete solitons exhibit poor or no mobility due to their strong pinning by the PN potential. Several ideas have been proposed to enhance the mobility for both one-dimensional [20] and two-dimensional [21] waveguide arrays, including also modulated nonlinearity [22], defects [23], PT symmetric couplers [24], etc.

The binding mechanism between solitons in optical fibers is a subject of interest from both the fundamental and applied points of view due to the increase of data rates in optical telecommunication [25]. Similarly, it is interesting to investigate the possibility of forming a bound state of two solitons in two-dimensional (2D) waveguide arrays. The present paper is building on our previous work [19] where we have shown that discrete solitons become highly mobile in 2D waveguide arrays with anisotropic coupling strengths. Specifically, our main objectives include: (i) studying the effect of the binding between the two solitons on their mobility, (ii) calculating the force and potential of interaction between the two solitons, (iii) calculating the PN potential for the two solitons and how the soliton-soliton interaction modulates it, and (iv) investigating the possibility that a robust stable bound state between two solitons exists.

The stability and dynamics of discrete solitons are well described by the discrete nonlinear Schrödinger equation (DNLSE), which is nonintegrable but can be solved using variational, perturbative, and numerical methods [26–32]. Using both numerical and variational calculations, we achieve all of the above-mentioned objectives, and specifically, we show that a robust unpinned soliton molecule indeed exists in anisotropic waveguides. Another interesting phenomenon is a soliton molecule *fission* where a bound state of two out-of-phase solitons suddenly splits into two solitons propagating away from each other.

The rest of the paper is organized as follows. In Sec. II we present the DNLSE model that describes the evolution of the solitons. In Sec. III, we solve the model numerically to obtain the equilibrium width and ground-state energy of the two solitons. In Sec. IV, we present a variational calculation and calculate the energy functional and the PN potential. In this section, we reproduce the equilibrium properties of the soliton molecules obtained numerically, calculate the PN potential, and the soliton-soliton interaction. In Sec. V, we investigate the soliton molecule and soliton fission in an anisotropic waveguide array. Finally, we end by summarizing our main results in Sec. VI.

II. MODEL EQUATION

The propagation of discrete solitons in two-dimensional waveguide arrays is described, within the tight-binding

*u.alkhawaja@uaeu.ac.ae

model [13], by the scaled 2D discrete nonlinear Schrödinger equation

$$i\frac{\partial}{\partial t}\Psi_{m,n} + (d_x\Psi_{m+1,n} + d_x\Psi_{m-1,n} + d_y\Psi_{m,n+1} + d_y\Psi_{m,n-1} - 2(d_x + d_y)\Psi_{m,n}) + \gamma|\Psi_{m,n}|^2\Psi_{m,n} = 0, \quad (1)$$

where $\Psi_{m,n}$ is the field envelope at site (m, n), γ is the strength of the nonlinearity, which is considered here to be positive in order to analyze bright solitons, and the coupling coefficients between waveguides in the horizontal and vertical directions are represented by d_x and d_y, respectively, and t corresponds to the distance along the waveguides. We have already used this model in [19] to study the stability and mobility of single 2D discrete solitons in isotropic and anisotropic waveguides. Here, we consider a soliton molecule instead of a single soliton in an anisotropic waveguide array such that the coupling between the waveguides along one direction is stronger than the other. There are three stationary 2D soliton types, known in the literature for the isotropic version of Eq. (1), which are named the site-centered (SC), bond-centered (BC), and hybrid solitons. Some references might use other names. As we have pointed out recently [19], for the anisotropic case the hybrid soliton splits into two different forms, namely, hybrid-X (HX) and hybrid-Y (HY). In principle, we can consider each soliton in the molecule to be any of these types. However, for simplicity, we consider both solitons to be the site-centered type.

The purpose of this work is to investigate the stability and mobility of such a discrete soliton molecule in 2D waveguide arrays. Specifically, we will investigate the effect of binding on mobility. It is established that a single 2D soliton exhibits very weak mobility in 2D waveguide arrays. The question we will address here is whether a 2D soliton molecule would be more mobile than a single soliton or not. The existence and mobility of the 2D solitons molecules will be investigated in both isotropic and anisotropic waveguide arrays. To that end, we consider, generally different horizontal and vertical coupling strengths. In reality, this can be easily realized by modulating the waveguide separations. In the following two sections, we investigate this problem first numerically and then variationally. The numerical calculation leads to the equilibrium width and ground-state energy. The variational calculation reproduces these results and helps to derive an analytical expression of the soliton-soliton and soliton-waveguide interaction potentials.

III. EQUILIBRIUM WIDTH AND ENERGY: NUMERICAL SOLUTION

In this section, we calculate the equilibrium properties of the soliton molecule and then study its mobility by solving the model Eq. (1) numerically. This will allow us to find the possible stable soliton molecule states. We employ the finite-difference method of Ref. [30] that is slightly modified to take into account the possibility of having an anisotropic waveguide array. We assume an $(L \times L)$-dimensional square

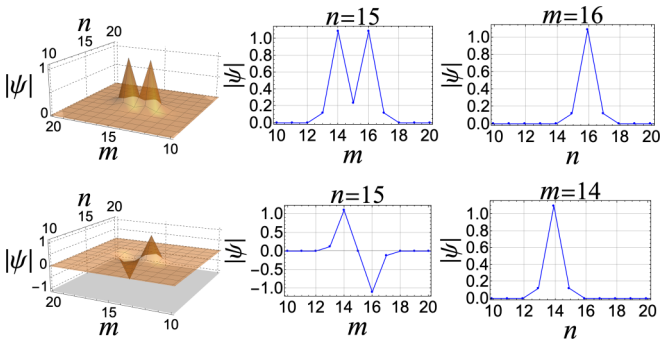

FIG. 1. In-phase (upper panel) and out-of-phase (lower panel) soliton molecule profiles obtained by numerical solution of Eq. (1) with isotropic waveguide array. The plots on the right-hand side show the two cross-section profiles. Parameters used: $L = 30$, $P = 2$, $\gamma = 4$, $d_x = d_y = 0.5$.

lattice. The initial condition is given in matrix form $[H]$ of the following type, namely,

$$[H]_{M,N} = 2\,d_x + 2\,d_y - \gamma|\Psi_{M,N}|^2, \quad (2)$$

$$[H]_{M+1,N} = [H]_{M-1,N} = -d_x, \quad (3)$$

$$[H]_{M,N+1} = [H]_{M,N-1} = -d_y, \quad (4)$$

where $M = m + (l-1)n$ and $N = n + (l-1)m$, $l = 1, 2, ...L$ for the square lattices of size $L \times L$. Solving the linear eigenvalue problem refines the prediction of $\Psi_{m,n}$ as the eigenfunction corresponding to the most negative eigenvalue. This procedure is repeated until the desired precision is obtained.

For the initial profile, one can in principle choose a combination of any soliton type out of the four types of stationary soliton profiles. Here, for the sake of simplicity, we choose only SC type trial functions as follows:

$$\Psi_{m,n} = A\left(e^{-\frac{(m-n_{1x})^2}{\eta_1^2} - \frac{(n-n_{1y})^2}{\eta_2^2}} + e^{-\frac{(m-n_{2x})^2}{\eta_1^2} - \frac{(n-n_{2y})^2}{\eta_2^2} + i\phi}\right), \quad (5)$$

where A is the normalization constant, and $n_{1x,1y}$ and $n_{2x,2y}$ are the coordinates peak positions of the first and second solitons, $\eta_{1,2}$ are the widths of the first and second soliton in horizontal and vertical directions, respectively, and ϕ is the phase difference between the two solitons.

We solve the model Eq. (1) using a trial function of the form given by Eq. (5) to find the two ground-state stationary soliton molecule states as shown in Figs. 1 and 2. In these figures the upper panel displays the in-phase stationary profiles for a combination of two solitons and the lower panel shows the out-of-phase profiles for an isotropic waveguide array. Considering anisotropic waveguide arrays by changing the coupling strength, such as, for instance, $dx = 2$ and $dy = 0.15$, leads to elongation of the width of the soliton molecule in one direction. A comparison of soliton cross sections in isotropic and anisotropic waveguides is shown in Fig. 3.

IV. VARIATIONAL CALCULATION

The advantage of using a variational calculation is to derive an analytical expression for Peierls-Nabarro (PN) potential

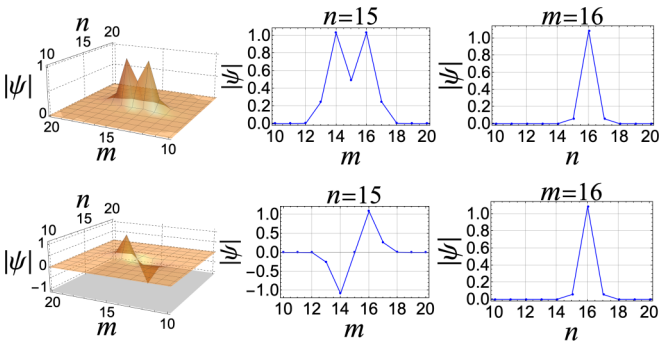

FIG. 2. In-phase (upper panel) and out-of-phase (lower panel) soliton molecule profiles obtained by numerical solution of Eq. (1) with anisotropic waveguide array. Parameters used are the same as for the isotropic case in Fig. 1 but with $d_x = 1.0$ and $d_y = 0.2$.

which helps us to calculate the barrier in both horizontal and vertical directions.

We start from the Lagrangian corresponding to Eq. (1), which takes the following form:

$$L = \sum_{m=-\infty}^{\infty}\sum_{n=-\infty}^{\infty}\left[\frac{i}{2}\left(\Psi_{m,n}\frac{\partial}{\partial t}\Psi^*_{m,n} - \Psi^*_{m,n}\frac{\partial}{\partial t}\Psi_{m,n}\right) - E\right], \tag{6}$$

where the dispersion and nonlinear terms define the energy functional

$$E = -\sum_{m=-\infty}^{\infty}\sum_{n=-\infty}^{\infty}\Big\{\Psi^*_{m,n}[d_x\,\Psi_{m-1,n} + d_x\,\Psi_{m+1,n} + d_y\Psi_{m,n-1} + d_y\Psi_{m,n+1} - 2(d_x + d_y)\Psi_{m,n}] + \frac{1}{2}\gamma|\Psi_{m,n}|^4\Big\}. \tag{7}$$

There are three kinds of trial functions which have been used widely in the literature to calculate the energy function, namely, (i) Gaussian, (ii) exponential, and (iii) secant function. As mentioned in [33], by using a secant trial function the summations in the Lagrangian cannot be performed in compact form and only asymptotic expressions can be obtained. This is not the case with exponential and Gaussian trial functions, where it is possible to perform the sums and generate a compact Lagrangian form. Here we use the Gaussian trial function since it results in simpler expressions and requires no prior assumptions on the location of the peak

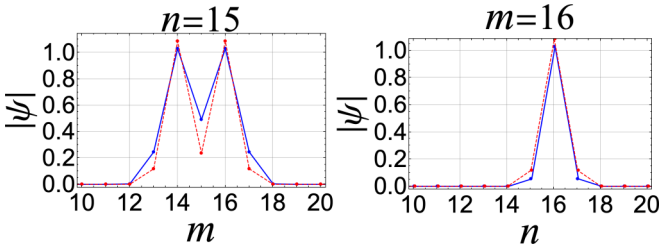

FIG. 3. Comparison between the cross sections of isotropic and anisotropic in-phase soliton-molecule profiles from Figs. 1 and 2. Dashed red and solid blue lines correspond to isotropic and anisotropic waveguide arrays, respectively.

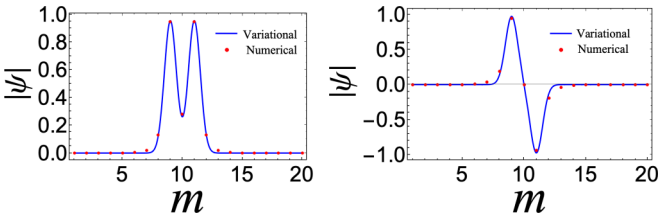

FIG. 4. In-phase and out-of-phase isotropic soliton molecules obtained by both numerical (red dots) and variational method (blue solid line) for the choice of parameters $L = 20$, $P = 2$, $\gamma = 4$, $d_x = d_y = 0.5$ with the assumption of $\phi = 0$ and π to achieve in-phase (left) and out-of-phase (right) solitons.

of the solitons. This enables us to consider the hopping of the soliton across the sites of the waveguide. The exponential trial function will be used only in Sec. V B to confirm the expression obtained for the potential of interaction in a soliton molecule obtained using the Gaussian trial function.

We start the variational calculation by normalizing the trial function given by Eq. (5) to the constant power P,

$$P = \sum_{m=-\infty}^{\infty}\sum_{n=-\infty}^{\infty}|\Psi_{m,n}|^2, \tag{8}$$

which gives A in terms of the elliptical function $\vartheta_3(x, y)$,

$$A = \frac{\sqrt{P}}{\sqrt{\frac{\pi}{2}}\sqrt{\eta_1\eta_2[A_1 + (A_2 + A_3)]}}, \tag{9}$$

where

$$A_1 = \frac{\vartheta_3(-n_{1x}\pi, X_1)\vartheta_3(-n_{1y}\pi, X_2)}{\exp\left(-\frac{{n_{1x}}^2+{n_{2x}}^2}{4{\eta_1}^2} - \frac{(n_{1y}-n_{2y})^2}{4\eta_2^2} - \frac{i\phi}{2}\right)},$$

$$A_2 = (1 + e^{2m\phi})\vartheta_3\left(-\frac{1}{2}(n_{1x} + n_{2x})\pi, X_1\right) \times \vartheta_3\left(-\frac{1}{2}(n_{1y} + n_{2y})\pi, X_2\right) \times \exp\left(-\frac{{n_{1x}}^2 - 4n_{1x}n_{2x} + {n_{2x}}^2}{2{\eta_1}^2} - \frac{(n_{1y} - n_{2y})^2}{2\eta_2^2} - i\phi\right),$$

$$A_3 = \frac{\vartheta_3(-n_{2x}\pi, X_1)\vartheta_3(-n_{2y}\pi, X_2)}{\exp\left(-\frac{{n_{1x}}^2+{n_{2x}}^2}{4{\eta_1}^2} - \frac{(n_{1y}-n_{2y})^2}{4\eta_2^2} - \frac{i\phi}{2}\right)},$$

and $X_1 = e^{-\frac{1}{2}\pi^2{\eta_1}^2}$ and $X_2 = e^{-\frac{1}{2}\pi^2{\eta_2}^2}$. We then calculated the energy functional using of the above normalized trial function, which is given in Appendix.

The variational and numerical equilibrium profiles of the isotropic waveguide array are shown in Fig. 4. The left and right subfigures display the isotropic soliton molecule profiles for in-phase, $\phi = 0$, and out-of-phase, $\phi = \pi$, cases, respectively. Here, we fixed both solitons on the x axis $n_{1y} = n_{2y} = 0$, fixed the first soliton at origin $n_{1x} = 0$, and left the position of the second soliton on the x axis, n_{2x}, to vary. The figures show that the variational and numerical profiles are in excellent agreement with each other.

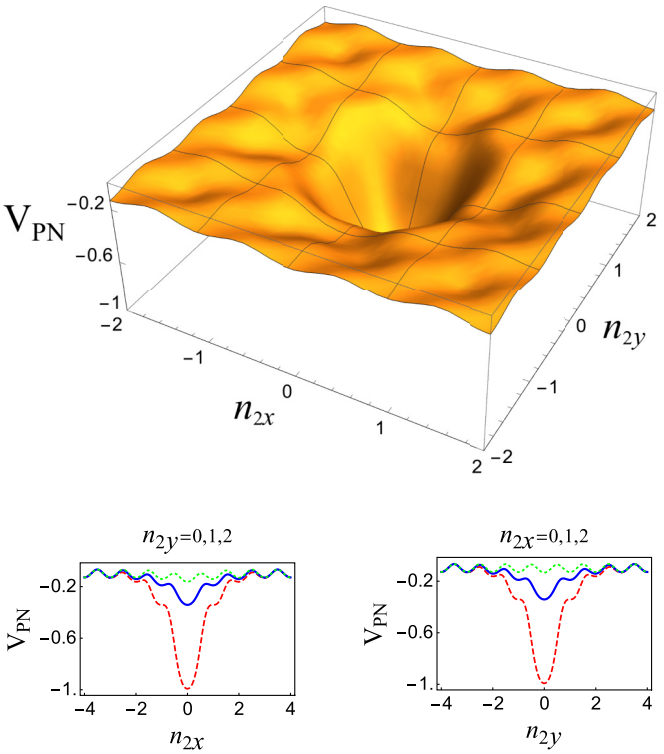

FIG. 5. In-phase PN potential for the isotropic case (upper panel) and the two cross sections of the PN potential (lower panel). The parameters used are $P = 2$, $\gamma = 4$, $n_{1x} = n_{1y} = 0$, $\eta_1 = \eta_{10}$ and $\eta_2 = \eta_{20}$, $d_x = d_y = 0.5$ with $\phi = 0$. Red dashed line corresponds to $n_{2y} = 0$ and $n_{2x} = 0$ for the left and right subfigures, respectively. Solid blue corresponds to $n_{2y} = 1$ and $n_{2x} = 1$, and dotted green corresponds to $n_{2y} = 2$ and $n_{2x} = 2$.

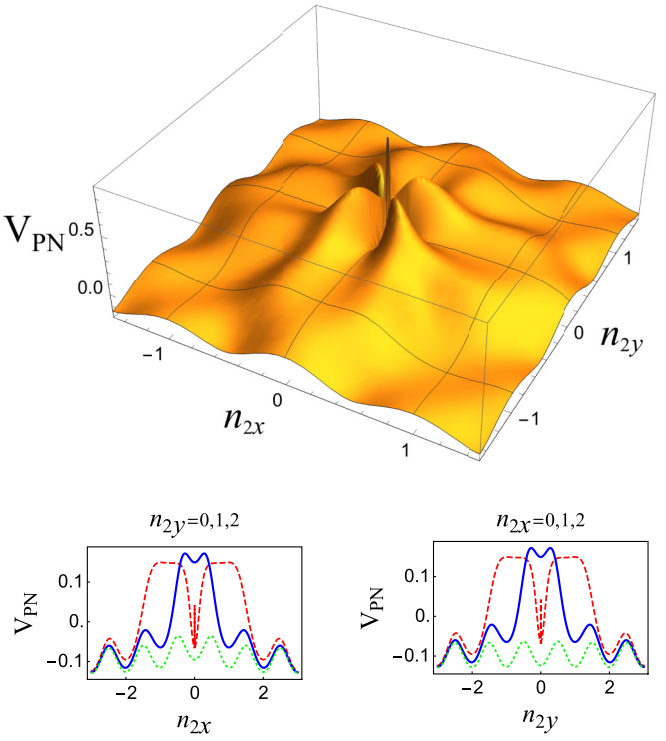

FIG. 6. Out-of-phase PN potential for the isotropic case (upper panel) and its two cross sections (lower panel). Parameters used are the same as in Fig. 5 but with $\phi = \pi$. Red dashed line corresponds to $n_{2y} = 0$ and $n_{2x} = 0$ for the left and right subfigures, respectively. Solid blue corresponds to $n_{2y} = 1$ and $n_{2x} = 1$, and dotted green corresponds to $n_{2y} = 2$ and $n_{2x} = 2$.

A. Equilibrium width and energy

At this stage, the energy functional is a function of the two soliton peak positions and widths, i.e., $E = E(n_{1x}, n_{1y}, n_{2x}, n_{2y}, \eta_1, \eta_2)$. To find the soliton equilibrium widths, the energy needs to be minimized with respect to η_1 and η_2:

$$\left.\frac{\partial E}{\partial \eta_1}\right|_{\eta_1=\eta_{10}} = 0, \quad \left.\frac{\partial E}{\partial \eta_2}\right|_{\eta_2=\eta_{20}} = 0, \tag{10}$$

where η_{10} and η_{20} are the equilibrium widths. We assume $\eta_2 = \eta_1$ and then minimize the energy with respect η_1. There are two possible schemes to achieve this: either by considering the trial function for a single soliton only or by fixing the first soliton at origin $n_{1x} = n_{1y} = 0$ while the second soliton is placed remotely: $n_{2x} = 0$ and $n_{2y} = \infty$. The equilibrium profiles for both schemes turns out to be the same, as it should be.

By substituting η_{10} and η_{20} in the ansatz function, we find the equilibrium profiles, and while substituting them into the energy functional we obtain the PN potential as a function of n_{2x} and n_{2y}. The profiles of PN potential for in-phase and out-of-phase solitons are displayed in Figs. 5 and 6, respectively. To generate these plots, we set one soliton at origin ($n_{1x} = 0$ and $n_{1y} = 0$) and thus we obtain the PN potential in terms of the coordinates of the second soliton, $V_{PN} = V_{PN}(n_{2x}, n_{2y})$.

The numerical diagonalization scheme of the system given by Eqs. (2)–(4) generates at once the whole spectrum of eigenenergies and eigenfunctions, including the ground state and excited states of the soliton molecule. This enables us to compare numerical ground-state energy with the variational one, as in Fig. 7. The variational calculation clearly captures the ground state of the soliton molecule for many soliton

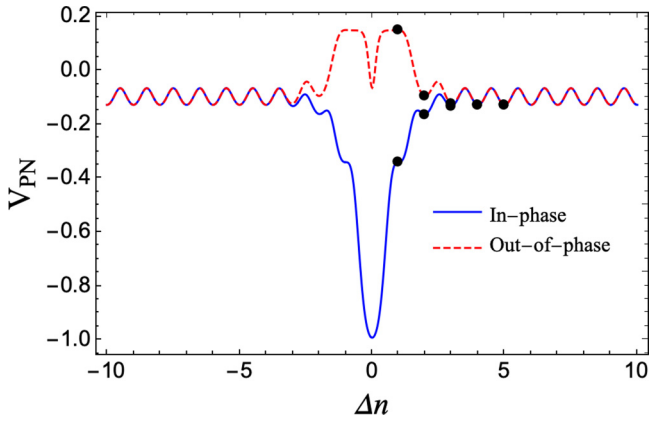

FIG. 7. The PN potential for separation of solitons calculated variationally for two choices of phases: in-phase (blue solid line) and out-of-phase (red dashed line). Numerically calculated points are presented by black dots for the choice of parameters $P = 2$, $\gamma = 4$, $d_x = d_y = 0.5$.

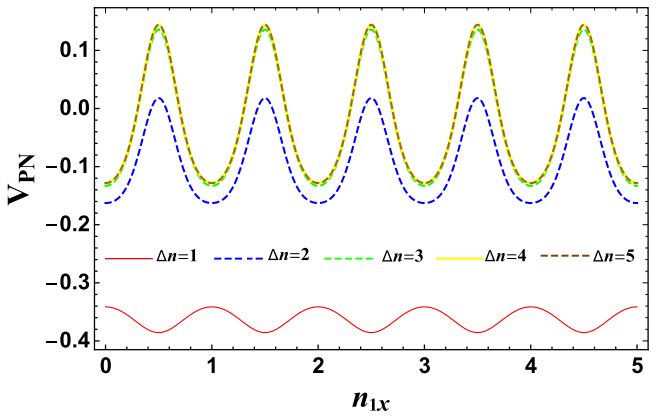

FIG. 8. The PN potential vs the molecule's position for different soliton separations $\Delta n = n_{2x} - n_{1x}$. The parameters used are $P = 2$, $\gamma = 4$, $n_{2x} = n_{2y} = 0$, $\eta_1 = \eta_{10}$, $\eta_2 = \eta_{20}$, $d_x = d_y = 0.5$.

separations. One can clearly notice in this figure the modulation brought by the interaction between solitons to the PN potential. When the two solitons are widely separated, the PN potential is periodic, as for single solitons. However, when the solitons are close, the PN potential acquires an additional potential well (barrier) for in-phase (out-of-phase) solitons.

B. Characteristics of PN potential

To study the role of binding on mobility, we investigate the dependence of the PN potential on the location of the molecule, its orientation with respect to the direction of motion, and bond length. We plot the PN potential for varying the molecule's center of mass with the soliton's separation, $\Delta n =$ 1, 2, 3, 4, and 5, as shown in Fig. 8. This figure indicates that the PN potential is lowest for the two solitons with the closest separation. By increasing the separation between the two solitons, the barrier of the potential increases. For separations $\Delta n \geqslant 3$, the PN potential remains the same. Consequently, separations $\Delta n > 2$ will not effect the PN potential, since the interaction between the two solitons becomes negligible. This figure suggests that, in principle, mobility should be enhanced for the two solitons with closest separation. However, numerical investigations show that solitons are immobile for this case due to the increase in the barrier height.

Now, we investigate the mobility in terms of the molecule's direction of movement. We considered two trajectories: (i) parallel to the molecule's axis and (ii) at 45° with respect to the molecule's axis. Figure 9 show that when the two solitons are moved in the diagonal direction, the PN barrier becomes higher and it is harder now to move the solitons.

C. Soliton-soliton interaction

The PN potential is the sum of the soliton-soliton interaction potential and the interaction between the solitons and the waveguide array

$$V_{PN} = V_{SS} + V_{PN}^{\infty}, \tag{11}$$

where V_{SS} is the soliton-soliton interaction and V_{PN}^{∞} is the limit of V_{PN} when the two solitons are widely separated such that their V_{SS} vanishes. We may thus calculate V_{SS} using, for instance,

$$V_{SS}(n_{2x}) = V_{PN}|_{\substack{n_{1y}=0\\ n_{2y}=0\\ n_{1x}=0}} - V_{PN}|_{\substack{n_{1y}=0\\ n_{2y}=0\\ n_{1x}\to\infty}} . \tag{12}$$

Figure 10 shows V_{SS} in terms of separation between solitons, namely, n_{2x}, since we have fixed one soliton at origin. While out-of-phase solitons repel, due to the potential barrier, the in-phase solitons attract and experience a molecular-type interaction potential.

In principle, the soliton-soliton interaction allows for the formation of a soliton molecule. However, the magnitude of the potential depth (bond strength) is in this case much smaller than the PN potential barrier. Therefore, binding will have no effect on the mobility or pinning of solitons. The concept of a soliton molecule in this case is excluded. On the other hand, we will show in the next section that when the two solitons are located at different waveguides with high anisotropy, the soliton-soliton interaction will be dominant and a stable soliton molecule forms.

V. ANISOTROPIC WAVEGUIDE ARRAYS

We have shown in a recent work that 2D solitons become mobile in anisotropic waveguides [19]. We have also shown in the present paper that binding between solitons in an isotropic waveguide has no effect on their mobility. Therefore, we consider soliton molecules in anisotropic waveguides, expecting the binding to enhance their mobility.

A. Equilibrium profiles and mobility

The PN potentials for an in-phase and out-of-phase combination of two solitons with anisotropic waveguide array is shown in Figs. 11 and 12, respectively. The figures show that mobility should be high in the horizontal direction compared to that in the vertical direction. By comparing the cross sections of Fig. 11 with Fig. 5, we can see that the PN potential is not periodic as it was in the isotropic case. The variational and numerical equilibrium profiles of the anisotropic waveguide are shown in Fig. 13. Agreement between the variational and numerical profiles is clear in this figure.

B. Formation of soliton molecule

We have already found that 2D soliton molecules are completely immobile in isotropic waveguide arrays [19]. Hence, the anisotropy was invoked and therefore we consider anisotropic waveguide array with coupling in the horizontal (x) direction to be much weaker than in the vertical (y) direction. With high anisotropy, the PN potential in the horizontal direction, V_{PNx}, is shown to be almost a monotonic potential well with a global minimum at zero separation between the two solitons, while the PN potential in the vertical direction, V_{PNy}, is oscillatory, as shown in Fig. 11. The cross sections of the PN potential shown in Fig. 11 indicate that if the two solitons are located at the same waveguide, they will coalesce.

Locating the solitons at different waveguides prevents them from coalescing due to the potential barrier existing between them. Nonetheless, the two solitons can still interact through the overlap of their tails across the waveguides. Therefore,

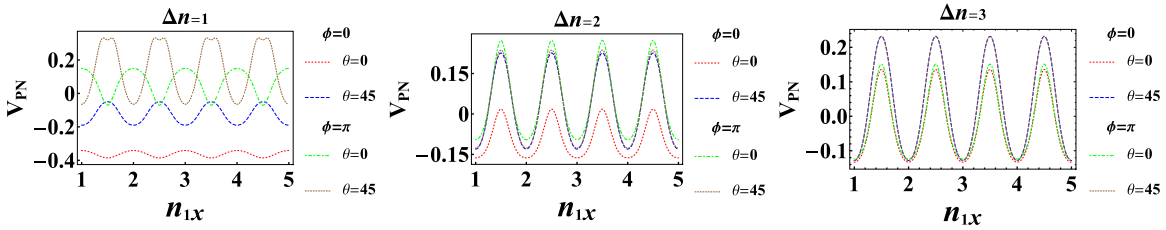

FIG. 9. The PN potential for two orientations [$\theta = 0$ (red dotted), $\theta = 45$ (blue dashed)] for in-phase $\phi = 0$ and [$\theta = 0$ (green dot dashed), $\theta = 45$ (brown tiny-dashed)] for out-of-phase $\phi = \pi$, respectively, with three different fixed separations $\Delta n = n_{2x} - n_{1x} = 1$ (left), $\Delta n = 2$ (middle), and $\Delta n = 3$ (right). Parameters used are $P = 2$, $\gamma = 4$, and $d_x = d_y = 0.5$.

while the two solitons will be completely mobile in the horizontal direction, they are restricted to move only along their respective waveguides. This results in a special kind of a soliton molecule where the stability is provided by the PN potential and energy exchange is provided by the soliton-soliton interaction. Comparing Figs. 11 and 12 shows that molecule formation is possible only for the in-phase solitons. Out-of-phase solitons are always expelled out of the waveguide because their force of interaction is expulsive.

Inspired by the above prediction of the variational calculation, we performed a numerical simulation of the two in-phase solitons separated initially by two waveguides in the y direction and by an arbitrary nonzero initial separation in the x direction. The dynamics of the solitons is then obtained by solving numerically the DNLSE, Eq. (1). The resulting dynamics is shown in Fig. 14. The two solitons oscillate around their center of mass, indicating the formation of a soliton bound state. The trajectories of the two solitons are shown in Fig. 15.

The potential of interaction between the two solitons can be obtained from their trajectories. By calculating the soliton separation $\Delta n(t) = n_{2x}(t) - n_{1x}(t)$ and differentiating it twice to obtain the force $F = \mu d^2/dt^2 \Delta n(t)$, where μ is the *reduced effective mass* of the two solitons, we then calculate the potential by integrating the force with respect to $\Delta n(t)$:

$$V = -\int_{\Delta n_{x_{\min}}}^{\Delta n_{x_{\max}}} F(\Delta n)\, d(\Delta n), \tag{13}$$

where $\Delta n_{\min}$ and $\Delta n_{\max}$ are the minimum and maximum soliton separation.

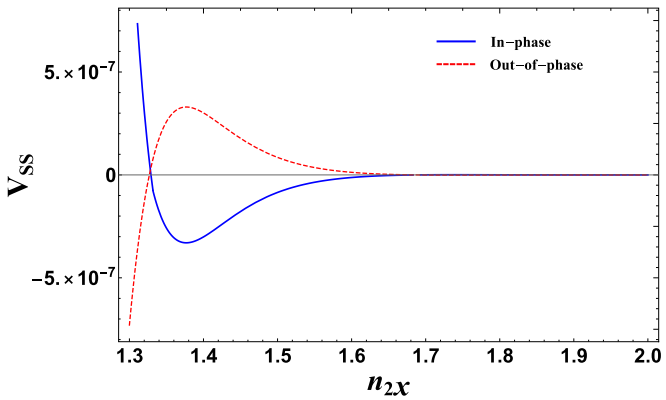

FIG. 10. The soliton-soliton interaction given by Eq. (12) for the choice of parameters $P = 2$, $\gamma = 17$, $d_x = d_y = 0.1$.

In Fig. 16, we show the potential calculated numerically from Eq. (1). The potential is parabolic and the force of interaction is linear. This indicates that the soliton molecule can be modeled by a classical system of two masses attached to a spring.

It will be constructive to compare the numerical potential with the variational one. This is performed using both a Gaussian ansatz, as given by Eq. (5), and an exponential ansatz given by

$$\Psi_{m,n} = A\left(e^{-\frac{|m-n_{1x}|}{\eta_1} - \frac{|n-n_{1y}|}{\eta_2}} + e^{-\frac{|m-n_{2x}|}{\eta_1} - \frac{|n-n_{2y}|}{\eta_2} + i\phi}\right). \tag{14}$$

Both trial functions lead to excellent agreement between the variational and numerical results, as Fig. 16 clearly shows.

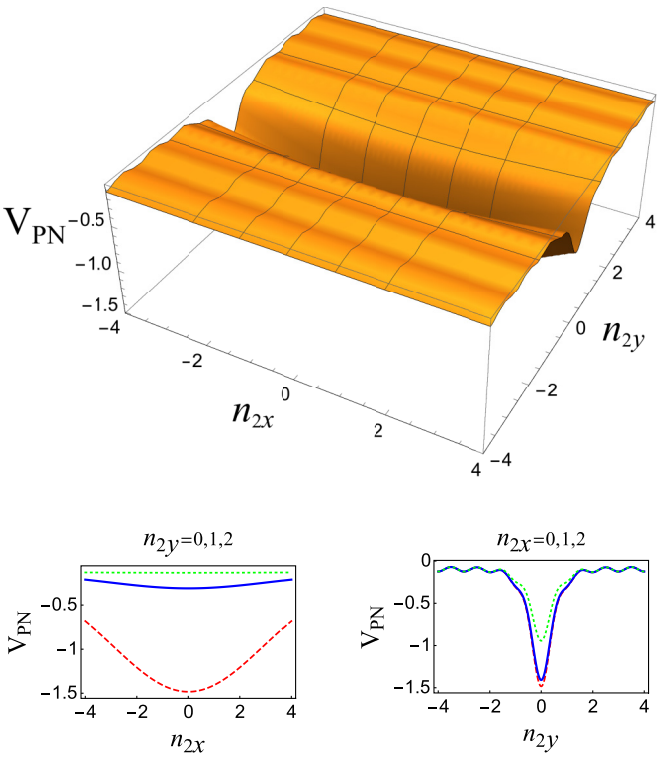

FIG. 11. In-phase PN potential for the anisotropic case (upper panel) and its two cross-section profiles (lower panel). The parameters used are $P = 2$, $\gamma = 4$, $n_{1x} = n_{1y} = 0$, $\eta_1 = \eta_{10} = 3.86$, and $\eta_2 = \eta_{20} = 0.760$, $d_x = 3$, $d_y = 0.15$ with $\phi = 0$. Red dashed line corresponds to $n_{2y} = 0$ and $n_{2x} = 0$ for the left and right subfigures, respectively. Solid blue corresponds to $n_{2y} = 1$ and $n_{2x} = 1$, and dotted green corresponds to $n_{2y} = 2$ and $n_{2x} = 2$.

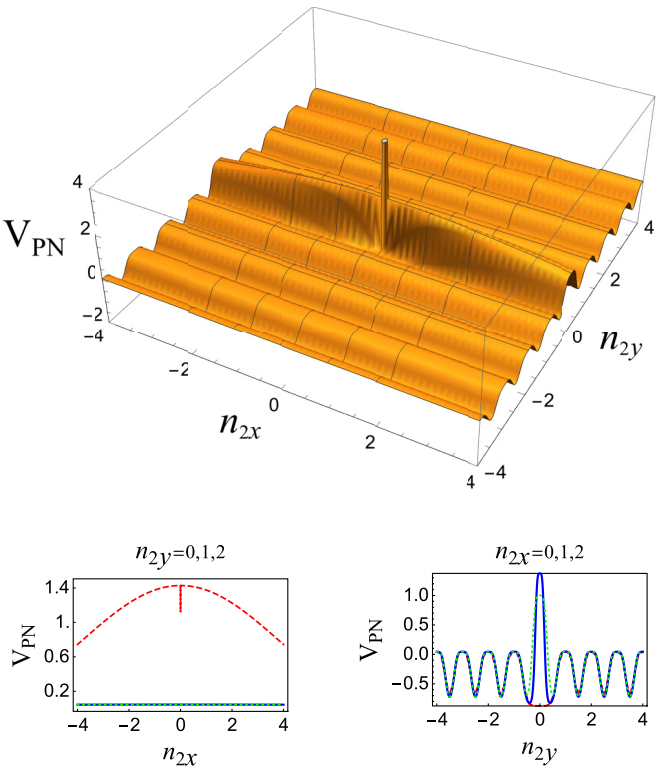

FIG. 12. Out-of-phase PN potential for the anisotropic case (upper panel) and its two cross-section profiles (lower panel). Parameters used are the same as in Fig. 11 but with $\phi = \pi$. Red dashed line corresponds to $n_{2y} = 0$ and $n_{2x} = 0$ for the left and right subfigures, respectively. Solid blue line corresponds to $n_{2y} = 1$ and $n_{2x} = 1$, and dotted green line corresponds to $n_{2y} = 2$ and $n_{2x} = 2$.

It should be noted that an arbitrary constant of integration resulting from the integration in Eq. (13) gave us the freedom to shift the numerical potential vertically in order to match the variational one. The curvature, on the other hand, fits naturally.

The above-mentioned analogy with the classical two-masses-spring system suggests the potential of interaction between the solitons to be parabolic in terms of their separation. Indeed, an accurate simplified analytical expression for the potential of interaction between the two solitons in terms of their separation, Δn, can be derived by expanding the energy functional to the quadratic order, as given by

$$V_{PN} = V_0 + \tfrac{1}{2}\, k\, \Delta n^2, \tag{15}$$

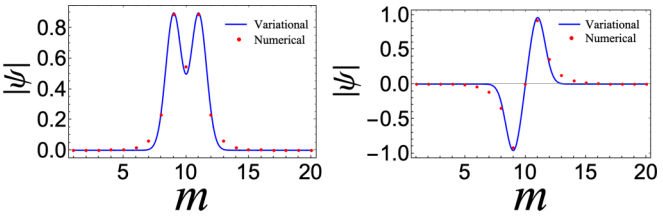

FIG. 13. In-phase and out-of-phase anisotropic soliton molecules obtained by both numerical (red dots) and variational method (blue solid line) for the choice of parameters $L = 20$, $P = 2$, $\gamma = 4$, $dx = 2$, and $dy = 0.2$ with $\phi = 0$ (left) and π (right).

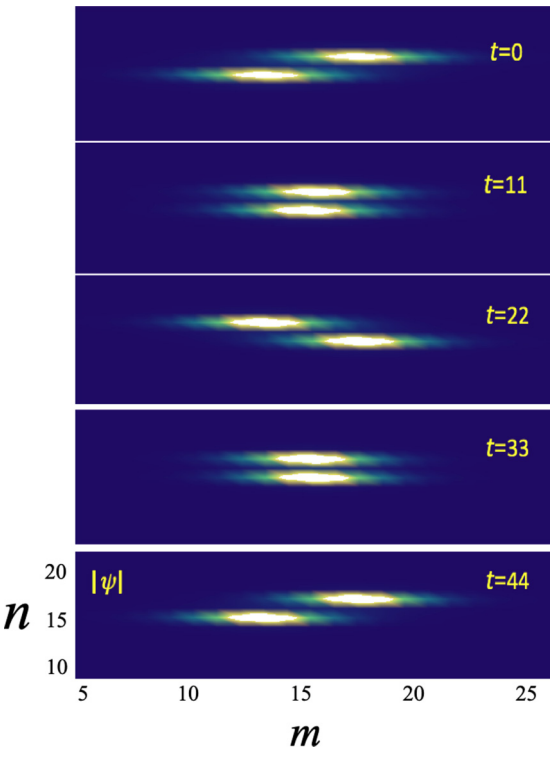

FIG. 14. Soliton molecule in anisotropic PN potential (in-phase) given in Fig. 11 along horizontal direction by means of numerical simulation of Eq. (1) and using the parameters $L = 30$, $P = 2$, $\gamma = 3$, $d_x = 3$, and $d_y = 0.15$. The two solitons are located initially at $n_{1x} = L/2 - 2$, $n_{2x} = L/2 + 2$, $n_{1y} = L/2$, $n_{2y} = L/2 + 2$.

where V_0 and k are given in terms of the parameters dx, dy, γ, and the soliton widths η_1 and η_2, as detailed in Appendix A 3.

In a classical system of two masses attached to a spring, the period of oscillation is given by $\tau = 2\pi\sqrt{\mu/k}$. The period of the soliton molecule can thus be estimated for a specific setup. For instance, for the parameters used to generate the soliton molecule shown in Fig. 14, the spring constant k can be calculated as given by Eq. (A12). The effective mass of a

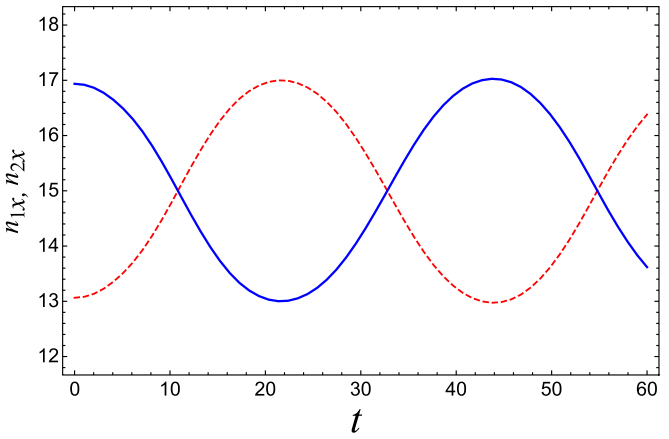

FIG. 15. Trajectories of the two solitons corresponding to the soliton molecule of Fig. 14.

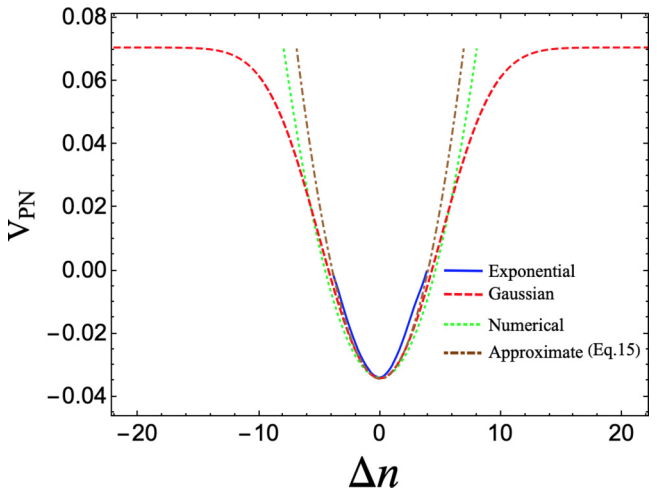

FIG. 16. The potential of interaction between two solitons in a soliton molecule obtained by: (i) the numerical solution of Eq. (1) and the trajectories of the two solitons in Fig. 15 (blue solid line), (ii) variational calculation using a Gaussian ansatz, Eq. (5), (red dashed line), and (iii) variational calculation using an exponential trial function, Eq. (14) (green dotted line). The dashed-dotted line corresponds to the simplified analytical expression Eq. (15). Parameters used are those of Fig. 14.

single soliton is given by the inverse of the second derivative of the energy with respect to the momentum, which in our case will be $2\,P\,d_x$. The reduced mass of the two solitons is thus $\mu = 1/2d_x$. For the parameters of Fig. 14, the estimate

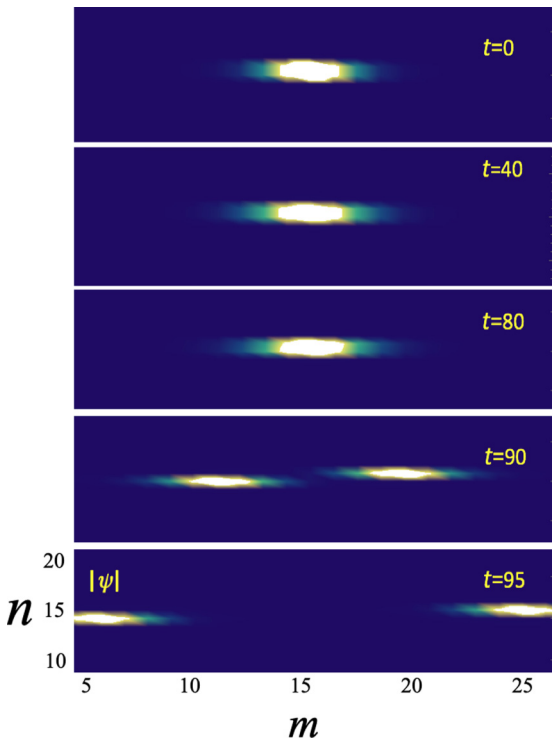

FIG. 17. Splitting of the soliton molecule. Parameters used: $P = 2$, $\gamma = 4$, $d_x = 3$, $d_y = 0.15$, $\eta_1 = 3.86$, and $\eta_2 = 0.76$, $\phi = \pi$, and initial positions $n_{2x} = n_{1x} = L/2$, $n_{1y} = L/2$, $n_{2y} = L/2 + 1$.

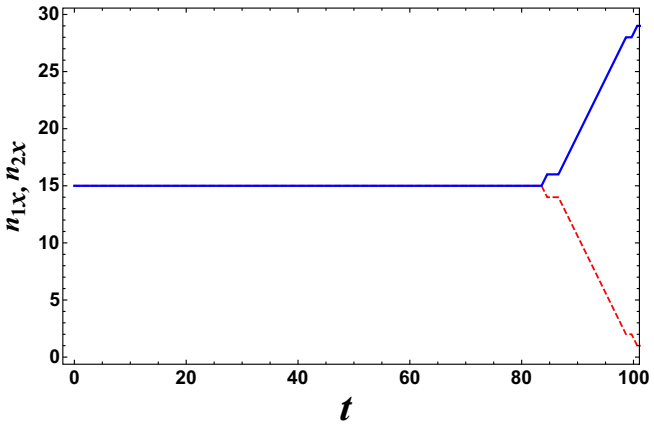

FIG. 18. Trajectories of the two solitons forming the soliton molecule of Fig. 17.

leads to $\tau \approx 39$, which is less the 10% off the numerical value of $\tau = 43.5$. This indicates that the force between the two solitons is indeed a Hooke-type of restoring force,

$$F = -k\,\Delta n. \tag{16}$$

It should be noted, however, that this applies for short soliton separations. For larger separations, the potential becomes constant and the force decays exponentially. This corresponds to the constant plateaus in the x cross section of the V_{PN} potential for large soliton separation, as shown in Figs. 16 and 19.

C. Soliton fission

Here, we consider a soliton molecule of two out-of-phase solitons placed at different waveguides. Basically, this is similar to the soliton molecule considered in the previous section but with out-of-phase solitons that are initially not separated from each other. Interestingly, we found this to be a metastable state with a long lifetime, after which it suddenly splits into two solitons propagating away from each other. We named this behavior *soliton fission*. Figure 17 shows the splitting of the soliton molecule. We can see that the solitons continue to coalesce up to $t = 80$, which is almost double the period of the soliton molecule of the previous case. The two solitons keep their coalescence as one soliton and exhibit only a small vibration in the amplitude. The soliton molecule then suddenly splits into two solitons propagating away from each other. Figure 18 shows the trajectories of the two solitons before and after splitting.

VI. CONCLUSIONS

We have used both numerical and variational calculations to obtain the equilibrium profiles and ground state of discrete two-soliton molecules in 2D waveguide arrays. Using a Gaussian variational trial function, Eq. (5), with six variational parameters corresponding to the coordinate peak positions and widths of the two solitons, we calculated the PN potential and the interaction potential between the solitons. We have investigated the mobility of the soliton molecule and found that binding does not enhance the mobility. Neither the bond

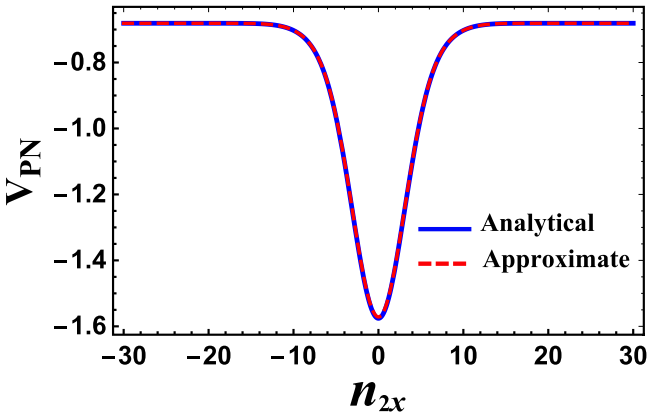

FIG. 19. The PN potential, given by Eq. (A1), is shown by the blue solid line, and the simplified form for the horizontal direction, given by Eq. (A8), is plotted by the red dashed line for the choice of parameters $P = 2$, $\gamma = 4$, $d_x = 3$, $d_y = 0.15$, $\eta_{10} = 3.86$, and $\eta_{20} = 0.76$ and $n_{2y} = 1$.

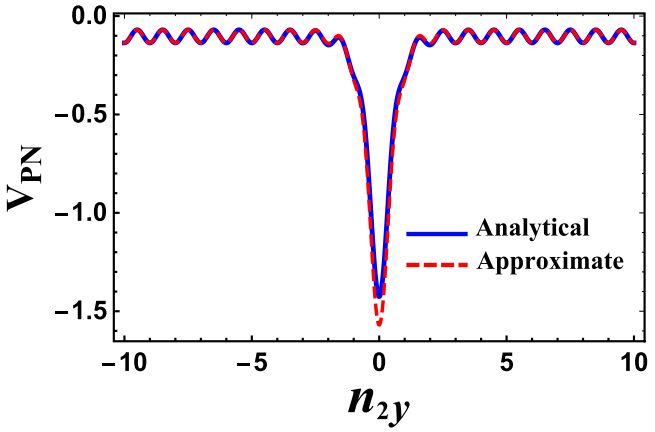

FIG. 20. The full and approximate PN potential given by Eqs. (A1) and (A9) are plotted using blue solid and red dashed lines, respectively, for the same parameters used in Fig. 19 but with $n_{2x} = 1$.

length nor the direction of the molecule's motion had a tangible effect on the mobility. We have shown the existence of stable discrete soliton molecules in two-dimensional waveguide arrays. Analogy was made to the classical diatomic model with linear restoring force. A simplified expression for the force and potential of interaction were derived, Eqs. (15) and (16). We have also found a unique behavior of a metastable state of a soliton molecule made of two out-of-phase solitons each place in a different waveguide. Such a molecule shows a sudden splitting into two solitons propagating away from each other. We believe our results will be valuable for all-optical applications using solitons to perform optical data processing.

ACKNOWLEDGMENT

The authors acknowledge the support of UAE University through Grants No. UPAR(7)-2015, No. UPAR(4)-2016, and No. UPAR(6)-2017.

APPENDIX: ENERGY FUNCTIONAL

1. Variational energy functional

The energy functional calculated using the trial function Eq. (5) in Eq. (7) is given by

$$E = \tfrac{1}{8}A^4\pi\gamma\eta_1\eta_2E_1 - A^2\big[-(d_x+d_y)\pi\eta_1\eta_2E_2 + \tfrac{1}{2}d_x\pi\eta_1\eta_2E_3 + \tfrac{1}{2}d_y\pi\eta_1\eta_2E_4\big], \tag{A1}$$

where

$$E_1 = -(4e^{2i\phi}+e^{4i\phi}+1)\vartheta_3\left(-\frac{1}{2}(n_{1x}+n_{2x})\pi, e^{-\frac{1}{4}\pi^2{\eta_1}^2}\right)\vartheta_3\left(-\frac{1}{2}(n_{1y}+n_{2y})\pi, e^{-\frac{1}{4}\pi^2{\eta_2}^2}\right)$$
$$\times \exp\left(-\frac{{n_{1x}}^2}{{\eta_1}^2}+\frac{2n_{1x}n_{2x}}{{\eta_1}^2}-\frac{2i{\eta_2}^2\phi+{n_{1y}}^2-2n_{1y}n_{2y}+{n_{2y}}^2}{{\eta_2}^2}-\frac{{n_{2x}}^2}{{\eta_1}^2}\right)-2(1+e^{2i\phi})$$
$$\times\left(\vartheta_3\left(-\frac{1}{4}(3n_{1x}+n_{2x})\pi, e^{-\frac{1}{4}\pi^2{\eta_1}^2}\right)\vartheta_3\left(-\frac{1}{4}(3n_{1y}+n_{2y})\pi, e^{-\frac{1}{4}\pi^2{\eta_2}^2}\right)+\vartheta_3\left(-\frac{1}{4}(n_{1x}+3n_{2x})\pi, e^{-\frac{1}{4}\pi^2{\eta_1}^2}\right)\right.$$
$$\left.\times\,\vartheta_3\left(-\frac{1}{4}(n_{1y}+3n_{2y})\pi, e^{-\frac{1}{4}\pi^2{\eta_2}^2}\right)\right)\exp\left(-\frac{1}{4{\eta_1}^2{\eta_2}^2}{\eta_2}^2\left(4i{\eta_1}^2\phi+3{n_{1x}}^2-6n_{1x}n_{2x}+3{n_{2x}}^2\right)+3{\eta_1}^2{n_{1y}}^2\right.$$
$$\left.-6{\eta_1}^2n_{1y}n_{2y}+3{\eta_1}^2{n_{2y}}^2\right)-\vartheta_3\left(-n_{1x}\pi, e^{-\frac{1}{4}\pi^2{\eta_1}^2}\right)\vartheta_3\left(-n_{1y}\pi, e^{-\frac{1}{4}\pi^2{\eta_2}^2}\right)-\vartheta_3\left(-n_{2x}\pi, e^{-\frac{1}{4}\pi^2{\eta_1}^2}\right)\vartheta_3\left(-n_{2y}\pi, e^{-\frac{1}{4}\pi^2{\eta_2}^2}\right), \tag{A2}$$

$$E_2 = (1+e^{2i\phi})\vartheta_3\left(-\frac{1}{2}(n_{1x}+n_{2x})\pi, e^{-\frac{1}{2}\pi^2{\eta_1}^2}\right)\vartheta_3\left(-\frac{1}{2}(n_{1y}+n_{2y})\pi, e^{-\frac{1}{2}\pi^2{\eta_2}^2}\right)\exp\left(\frac{n_{1x}n_{2x}}{{\eta_1}^2}+\frac{1}{2}\left(-\frac{{n_{1x}}^2}{{\eta_1}^2}-\frac{(n_{1y}-n_{2y})^2}{{\eta_2}^2}\right.\right.$$
$$\left.\left.-\frac{{n_{2x}}^2}{{\eta_1}^2}-2i\phi\right)\right)+\vartheta_3\left(-n_{1x}\pi, e^{-\frac{1}{2}\pi^2{\eta_1}^2}\right)\vartheta_3\left(-n_{1y}\pi, e^{-\frac{1}{2}\pi^2{\eta_2}^2}\right)+\vartheta_3\left(-n_{2x}\pi, e^{-\frac{1}{2}\pi^2{\eta_1}^2}\right)\vartheta_3\left(-n_{2y}\pi, e^{-\frac{1}{2}\pi^2{\eta_2}^2}\right), \tag{A3}$$

$$E_3 = e^{-\frac{1}{2\eta_1^2}}\Big(\vartheta_3\Big(-\frac{1}{2}(2n_{1x}+1)\pi, e^{-\frac{1}{2}\pi^2\eta_1^2}\Big)\vartheta_3\big(-n_{1y}\pi, e^{-\frac{1}{2}\pi^2\eta_2^2}\big) + \vartheta_3\Big(\frac{\pi}{2}-n_{1x}\pi, e^{-\frac{1}{2}\pi^2\eta_1^2}\Big)\vartheta_3\big(-n_{1y}\pi, e^{-\frac{1}{2}\pi^2\eta_2^2}\big)$$
$$+\vartheta_3\Big(-\frac{1}{2}(2n_{2x}+1)\pi, e^{-\frac{1}{2}\pi^2\eta_1^2}\Big)\vartheta_3\big(-n_{2y}\pi, e^{-\frac{1}{2}\pi^2\eta_2^2}\big) + \vartheta_3\Big(\frac{\pi}{2}-n_{2x}\pi, e^{-\frac{1}{2}\pi^2\eta_1^2}\Big)\vartheta_3\big(-n_{2y}\pi, e^{-\frac{1}{2}\pi^2\eta_2^2}\big)\Big)$$
$$+\big(e^{\frac{n_{1x}(n_{2y}+2)}{\eta_1^2}} + e^{\frac{(n_{1x}+2)n_{2x}}{\eta_1^2}+2i\phi}\big)\Big(\vartheta_3\Big(-\frac{1}{2}(n_{1x}+n_{2x}-1)\pi, e^{-\frac{1}{2}\pi^2\eta_1^2}\Big)\vartheta_3\Big(-\frac{1}{2}(n_{1y}+n_{2y})\pi, e^{-\frac{1}{2}\pi^2\eta_2^2}\Big)$$
$$+\vartheta_3\Big(-\frac{1}{2}(n_{1x}+n_{2x}+1)\pi, e^{-\frac{1}{2}\pi^2\eta_1^2}\Big)\vartheta_3\Big(-\frac{1}{2}(n_{1y}+n_{2y})\pi, e^{-\frac{1}{2}\pi^2\eta_2^2}\Big)\Big)\exp\Big(\frac{1}{2}\Big(-\frac{{n_{1x}}^2+2n_{1x}+(n_{2x}+1)^2}{{\eta_1}^2}$$
$$-\frac{2i\eta_2{}^2\phi+{n_{1y}}^2-2n_{1y}n_{2y}+{n_{2y}}^2}{{\eta_2}^2}\Big)\Big), \tag{A4}$$

$$E_4 = e^{-\frac{1}{2\eta_2^2}}\Big(\vartheta_3\big(-n_{1x}\pi, e^{-\frac{1}{2}\pi^2\eta_1^2}\big)\Big(\vartheta_3\Big(-\frac{1}{2}(2n_{1y}+1)\pi, e^{-\frac{1}{2}\pi^2\eta_2^2}\Big)+\vartheta_3\Big(\frac{\pi}{2}-n_{1y}\pi, e^{-\frac{1}{2}\pi^2\eta_2^2}\Big)\Big)+\vartheta_3\big(-n_{2x}\pi, e^{-\frac{1}{2}\pi^2\eta_1^2}\big)$$
$$\times\Big(\vartheta_3\Big(-\frac{1}{2}(2n_{2y}+1)\pi, e^{-\frac{1}{2}\pi^2\eta_2^2}\Big)+\vartheta_3\Big(\frac{\pi}{2}-n_{2y}\pi, e^{-\frac{1}{2}\pi^2\eta_2^2}\Big)\Big)\Big)+\vartheta_3\Big(-\frac{1}{2}(n_{1x}+n_{2x})\pi, e^{-\frac{1}{2}\pi^2\eta_1^2}\Big)$$
$$\times\exp\Big(\frac{1}{2}\Big(-\frac{(n_{1x}-n_{2x})^2}{{\eta_1}^2}-\frac{2i\eta_2{}^2\phi+{n_{1y}}^2+2n_{1y}(n_{2y}+1)+{n_{2y}}^2+2n_{2y}+1}{{\eta_2}^2}\Big)\Big)\Big(\big(e^{\frac{2n_{1y}(n_{2y}+1)}{\eta_2^2}}+e^{\frac{2(i\eta_2{}^2\phi+n_{1y}n_{2y}+n_{2y})}{\eta_2^2}}\big)$$
$$\times\vartheta_3\Big(-\frac{1}{2}(n_{1y}+n_{2y}-1)\pi, e^{-\frac{1}{2}\pi^2\eta_2^2}\Big)\exp\Big(\frac{1}{2}\Big(-\frac{{n_{1x}}^2+{n_{2x}}^2}{{\eta_1}^2}-\frac{2i\eta_2{}^2\phi+{n_{1y}}^2+2n_{1y}(n_{2y}+1)+{n_{2y}}^2+2n_{2y}+1}{{\eta_2}^2}\Big)\Big)$$
$$+\big(e^{\frac{2(n_{1y}+1)n_{2y}}{\eta_2^2}}+e^{\frac{2(i\eta_2{}^2\phi+n_{1y}n_{2y}+n_{1y})}{\eta_2^2}}\big)\vartheta_3\Big(-\frac{1}{2}(n_{1y}+n_{2y}+1)\pi, e^{-\frac{1}{2}\pi^2\eta_2^2}\Big)\exp\Big(\frac{1}{2}\Big(-\frac{{n_{1x}}^2+{n_{2x}}^2}{{\eta_1}^2}$$
$$-\frac{2i\eta_2{}^2\phi+{n_{1y}}^2+2n_{1y}(n_{2y}+1)+{n_{2y}}^2+2n_{2y}+1}{{\eta_2}^2}\Big)\Big)\Big)\Big). \tag{A5}$$

2. Simplified PN potential

The above full form of potential, Eq. (A1), can be simplified by expanding in powers of the small quantities $e^{-\pi^2\eta_1^2/4}$ and $e^{-\pi^2\eta_2^2/4}$ as follows:

$$V_{PNx} = -\tfrac{1}{4}\pi\eta_1\eta_2 e^{\frac{2n_{2y}}{\eta_2^2}}\Big[4d_x\big(-2e^{-\frac{{n_{2x}}^2}{2\eta_1^2}-\frac{n_{2y}(n_{2y}+4)}{2\eta_2^2}}+e^{-\frac{(n_{2x}-1)^2}{2\eta_1^2}-\frac{n_{2y}(n_{2y}+4)}{2\eta_2^2}}+e^{-\frac{(n_{2x}+1)^2}{2\eta_1^2}-\frac{n_{2y}(n_{2y}+4)}{2\eta_2^2}}+2e^{-\frac{1}{2\eta_1^2}-\frac{2n_{2y}}{\eta_2^2}}-2e^{-\frac{2n_{2y}}{\eta_2^2}}\big)$$
$$+d_y\big(4e^{-\frac{{n_{2x}}^2}{2\eta_1^2}-\frac{(n_{2y}+1)^2}{2\eta_2^2}}-8e^{-\frac{{n_{2x}}^2}{2\eta_1^2}-\frac{n_{2y}(n_{2y}+4)}{2\eta_2^2}}-8e^{-\frac{2n_{2y}}{\eta_2^2}}+8e^{-\frac{4n_{2y}+1}{2\eta_2^2}}\big)+3\big(3e^{-\frac{{n_{2x}}^2}{\eta_1^2}-\frac{n_{2y}(n_{2y}+2)}{\eta_2^2}}+4e^{-\frac{3{n_{2x}}^2}{4\eta_1^2}-\frac{n_{2y}(3n_{2y}+8)}{4\eta_2^2}}$$
$$+e^{-\frac{2n_{2y}}{\eta_2^2}}+e^{-\frac{1}{4}\pi^2\eta_2{}^2-\frac{2n_{2y}}{\eta_2^2}}\big)+18\cos(\pi n_{2y})e^{-\frac{\pi^2\eta_2{}^2}{4}-\frac{{n_{2x}}^2}{\eta_1^2}-\frac{n_{2y}(n_{2y}+2)}{\eta_2^2}}+3e^{-\frac{1}{4}\pi^2\eta_2{}^2-\frac{2n_{2y}}{\eta_2^2}}\cos(2\pi n_{2y})\Big] \tag{A6}$$

and

$$V_{PNy} = -\frac{1}{4}\pi\eta_1\eta_2 e^{\frac{2n_{2y}}{\eta_2^2}}\Big[4d_x\big(-2e^{-\frac{{n_{2x}}^2}{2\eta_1^2}-\frac{n_{2y}(n_{2y}+4)}{2\eta_2^2}}+2e^{-\frac{1}{2\eta_1^2}-\frac{2n_{2y}}{\eta_2^2}}-2e^{-\frac{2n_{2y}}{\eta_2^2}}+2e^{-\frac{n_{2y}(n_{2y}+4)}{2\eta_2^2}}\big)+d_y\big(8e^{-\frac{4n_{2y}+1}{2\eta_2^2}}-8e^{-\frac{2n_{2y}}{\eta_2^2}}\big)$$
$$+3\big(e^{-\frac{2n_{2y}}{\eta_2^2}}+3e^{-\frac{n_{2y}(n_{2y}+2)}{\eta_2^2}}+4e^{-\frac{n_{2y}(3n_{2y}+8)}{4\eta_2^2}}+e^{-\frac{1}{4}\pi^2\eta_2{}^2-\frac{2n_{2y}}{\eta_2^2}}\big)+12e^{\frac{1}{4}(-\pi^2\eta_2{}^2-\frac{n_{2y}(3n_{2y}+8)}{\eta_2^2})}\cos\Big(\frac{\pi n_{2y}}{2}\Big)$$
$$+18e^{-\frac{1}{4}\pi^2\eta_2{}^2-\frac{n_{2y}(n_{2y}+2)}{\eta_2^2}}\cos(\pi n_{2y})+12e^{\frac{1}{4}(-\pi^2\eta 2^2-\frac{n_{2y}(3n_{2y}+8)}{\eta_2^2})}\cos\Big(\frac{3\pi n_{2y}}{2}\Big)+3e^{-\frac{1}{4}\pi^2\eta_2{}^2-\frac{2n_{2y}}{\eta_2^2}}\cos(2\pi n_{2y})\Big], \tag{A7}$$

where V_{PNx} and V_{PNy} are the V_{PN} in the horizontal and vertical directions, respectively.

To further simplify this expression, we consider a highly anisotropic waveguide such as $d_x = 3$, $d_y = 0.15$. The equilibrium widths $\eta_{10,20}$ are then calculated by minimizing the potential with respect to the widths $\eta_{1,2}$, which gives $\eta_{10} = 3.86$, $\eta_{20} = 0.76$. This further simplifies the potential as follows:

$$V_{PNx} = c_1 - c_2(e^{2c_3n_{2x}}+1)e^{-n_{2x}(c_3+c_4n_{2x})} - c_5e^{c_3{n_{2x}}^2} + c_8e^{-c_4{n_{2x}}^2} - c_6e^{c_7{n_{2x}}^2}, \tag{A8}$$

where

$$c_1 = -6.810\,08, \quad c_2 = 11.249\,948, \quad c_3 = -0.067\,11, \quad c_4 = 0.033\,55, \quad c_5 = 1.905\,72, \quad c_6 = 7.546\,59,$$
$$c_7 = -0.050\,33, \quad c_8 = 23.048\,72$$

and

$$V_{PNy} = -c_1 + e^{n_{2y}(c_2 - c_3 n_{2y})}(c_4 - c_5\cos(\pi n_{2y})) + e^{n_{2y}(c_2 - c_6 n_{2y})}\left(c_7 - c_8\cos\left(\frac{\pi n_{2y}}{2}\right) - c_8\cos\left(\frac{3\pi n_{2y}}{2}\right)\right) - c_9\cos(2\pi n_{2y}),$$
$$c_1 = -5.147\,94, \quad c_2 = 8.881\,78x10^{-16}, \quad c_3 = 1.7313, \quad c_4 = -20.736\,39, \quad c_5 = 9.972\,85, \quad c_6 = 1.298\,47,$$
$$c_7 = -27.648\,52, \quad c_8 = 6.648\,56, \quad c_9 = 1.662\,14. \tag{A9}$$

In Figs. 19 and 20 we plot the approximate and full potential to see that they still agree very well.

3. V_{PN} for soliton molecule

The variational energy functional Eq. (A1) can be simplified for the special case of a soliton molecule where one soliton is restricted to move along the waveguide $n_{1y} = -1$ and the other soliton moves along the waveguide $n_{2y} = 1$, and thus the separation between the two solitons is essentially determined by $\Delta n = n_{2x} - n_{1x}$. The energy functional is therefore given in terms of the soliton separation as

$$\begin{aligned}
V_{PN} = \frac{1}{D} P\Bigg(&2e^{\frac{1}{2}(-\frac{2\Delta n+1}{\eta_1^2}-\frac{5}{\eta_2^2})}\Bigg(2\vartheta_3\left(0, e^{-\frac{1}{2}\pi^2\eta_1^2}\right)\vartheta_3\left(0, e^{-\frac{1}{2}\pi^2\eta_2^2}\right) + e^{\frac{\Delta n^2}{2\eta_1^2}+\frac{2}{\eta_2^2}}\Bigg(\vartheta_3\left(-\pi, e^{-\frac{1}{2}\pi^2\eta_2^2}\right)\vartheta_3\left(-\frac{\pi\Delta n}{2}, e^{-\frac{1}{2}\pi^2\eta_1^2}\right)\\
&+\vartheta_3\left(\pi, e^{-\frac{1}{2}\pi^2\eta_2^2}\right)\vartheta_3\left(\frac{\pi\Delta n}{2}, e^{-\frac{1}{2}\pi^2\eta_1^2}\right)\Bigg)\Bigg)\Bigg(-e^{\frac{2\Delta n+1}{2\eta_1^2}}\vartheta\Big(0, e^{-\frac{1}{2}\pi^2\eta_1^2}\Big)\Bigg(d_y\left(1+e^{\frac{4}{\eta_2^2}}\right)\Bigg(\vartheta_3\left(-\frac{\pi}{2}, e^{-\frac{1}{2}\pi^2\eta_2^2}\right)\\
&+\vartheta_3\left(\frac{\pi}{2}, e^{-\frac{1}{2}\pi^2\eta_2^2}\right)\Bigg) - 4(d_x+d_y)\,e^{\frac{5}{2\eta_2^2}}\vartheta_3\left(0, e^{-\frac{1}{2}\pi^2\eta_2^2}\right)\Bigg) - e^{\frac{5}{2\eta_2^2}}\Bigg(d_x\left(1+e^{\frac{2\Delta n}{\eta_1^2}}\right)\vartheta_3\left(0, e^{-\frac{1}{2}\pi^2\eta_2^2}\right)\Bigg(\vartheta_3\left(-\frac{\pi}{2}, e^{-\frac{1}{2}\pi^2\eta_1^2}\right)\\
&+\vartheta_3\left(\frac{\pi}{2}, e^{-\frac{1}{2}\pi^2\eta_1^2}\right)\Bigg) + e^{\frac{1}{2}(\frac{\Delta n(\Delta n+2)}{\eta_1^2}+\frac{3}{\eta_2^2})}\Bigg(d_y e^{\frac{1}{2\eta_1^2}}\vartheta_3\left(-\frac{3\pi}{2}, e^{-\frac{1}{2}\pi^2\eta_2^2}\right)\vartheta_3\left(-\frac{\pi\Delta n}{2}, e^{-\frac{1}{2}\pi^2\eta_1^2}\right) - 2d_x e^{\frac{1}{2}(\frac{1}{\eta_2^2}+\frac{1}{\eta_1^2})}\\
&\times\vartheta_3\left(-\pi, e^{-\frac{1}{2}\pi^2\eta_2^2}\right)\vartheta_3\left(-\frac{\pi\Delta n}{2}, e^{-\frac{1}{2}\pi^2\eta_1^2}\right) - 2d_y e^{\frac{1}{2}(\frac{1}{\eta_2^2}+\frac{1}{\eta_1^2})}\vartheta_3\left(-\pi, e^{-\frac{1}{2}\pi^2\eta_2^2}\right)\vartheta_3\left(-\frac{\pi\Delta n}{2}, e^{-\frac{1}{2}\pi^2\eta_1^2}\right)\\
&+d_y e^{\frac{1}{2\eta_1^2}}\vartheta_3\left(-\frac{\pi}{2}, e^{-\frac{1}{2}\pi^2\eta_2^2}\right)\vartheta_3\left(-\frac{\pi\Delta n}{2}, e^{-\frac{1}{2}\pi^2\eta_1^2}\right) + d_y e^{\frac{1}{2\eta_1^2}}\vartheta_3\left(\frac{\pi}{2}, e^{-\frac{1}{2}\pi^2\eta_2^2}\right)\vartheta_3\left(\frac{\pi\Delta n}{2}, e^{-\frac{1}{2}\pi^2\eta_1^2}\right)\\
&+d_y e^{\frac{1}{2\eta_1^2}}\vartheta_3\left(\frac{3\pi}{2}, e^{-\frac{1}{2}\pi^2\eta_2^2}\right)\vartheta_3\left(\frac{\pi\Delta n}{2}, e^{-\frac{1}{2}\pi^2\eta_1^2}\right) + d_x e^{\frac{1}{2\eta_2^2}}\vartheta_3\left(-\pi, e^{-\frac{1}{2}\pi^2\eta_2^2}\right)\vartheta_3\left(-\frac{1}{2}\pi(\Delta n+1), e^{-\frac{1}{2}\pi^2\eta_1^2}\right)\\
&+e^{\frac{1}{2\eta_2^2}}\vartheta_3\left(\pi, e^{-\frac{1}{2}\pi^2\eta_2^2}\right)\Bigg(d_x\vartheta_3\left(\frac{1}{2}\pi(\Delta n-1), e^{-\frac{1}{2}\pi^2\eta_1^2}\right) - 2(d_x+d_y)e^{\frac{1}{2\eta_1^2}}\vartheta_3\left(\frac{\pi\Delta n}{2}, e^{-\frac{1}{2}\pi^2\eta_1^2}\right)\\
&+d_x\vartheta_3\left(\frac{1}{2}\pi(\Delta n+1), e^{-\frac{1}{2}\pi^2\eta_1^2}\right)\Bigg) + d_x e^{\frac{1}{2\eta_2^2}}\vartheta_3\left(-\pi, e^{-\frac{1}{2}\pi^2\eta_2^2}\right)\vartheta_3\left(\frac{1}{2}(\pi-\pi\Delta n), e^{-\frac{1}{2}\pi^2\eta_1^2}\right)\Bigg)\Bigg)\Bigg)\\
&-\frac{1}{\pi\eta_1\eta_2}P\gamma\Bigg(6\vartheta_3\left(0, e^{-\frac{1}{4}\pi^2\eta_1^2}\right)\vartheta_3\left(0, e^{-\frac{1}{4}\pi^2\eta_2^2}\right) + e^{\frac{\Delta n^2}{4\eta_1^2}+\frac{1}{\eta_2^2}}\Bigg(e^{\frac{3\Delta n^2}{4\eta_1^2}+\frac{3}{\eta_2^2}}\vartheta_3\left(-\pi, e^{-\frac{1}{4}\pi^2\eta_2^2}\right)\vartheta_3\left(-\frac{\pi\Delta n}{2}, e^{-\frac{1}{4}\pi^2\eta_1^2}\right)\\
&+4\vartheta_3\left(-\frac{\pi}{2}, e^{-\frac{1}{4}\pi^2\eta_2^2}\right)\vartheta_3\left(-\frac{\pi\Delta n}{4}, e^{-\frac{1}{4}\pi^2\eta_1^2}\right) + 4\vartheta_3\left(\frac{\pi}{2}, e^{-\frac{1}{4}\pi^2\eta_2^2}\right)\vartheta_3\left(\frac{\pi\Delta n}{4}, e^{-\frac{1}{4}\pi^2\eta_1^2}\right) + e^{\frac{3\Delta n^2}{4\eta_1^2}+\frac{3}{\eta_2^2}}\\
&\times\vartheta_3\left(\pi, e^{-\frac{1}{4}\pi^2\eta_2^2}\right)\vartheta_3\left(\frac{\pi\Delta n}{2}, e^{-\frac{1}{4}\pi^2\eta_1^2}\right)\Bigg)\Bigg)\Bigg),
\end{aligned}$$

where,

$$\begin{aligned}
D = 2\Bigg(&2\vartheta_3\left(0, e^{-\frac{1}{2}\pi^2\eta_1^2}\right)\vartheta_3\left(0, e^{-\frac{1}{2}\pi^2\eta_2^2}\right) + e^{\frac{\Delta n^2}{2\eta_1^2}+\frac{2}{\eta-2^2}}\Bigg(\vartheta_3\left(-\pi, e^{-\frac{1}{2}\pi^2\eta_2^2}\right)\vartheta_3\left(-\frac{\pi\Delta n}{2}, e^{-\frac{1}{2}\pi^2\eta_1^2}\right) + \vartheta_3\left(\pi, e^{-\frac{1}{2}\pi^2\eta_2^2}\right)\\
&\times\vartheta_3\left(\frac{\pi\Delta n}{2}, e^{-\frac{1}{2}\pi^2\eta_1^2}\right)\Bigg)\Bigg)^2.
\end{aligned}$$

For highly anisotropic waveguides the soliton width in the x direction is at least more than several waveguides and the soliton width in the y direction is less than or of the order of a one waveguide. Consequently, the quantity $e^{-\pi^2\eta_1^2/4}$ is very small and

hence

$$\vartheta_3\left(n\,\pi, e^{-\pi^2\eta_1^2/4}\right) \approx 1, \tag{A10}$$

with arbitrary real n. On the other hand, the $\vartheta_3(n\,\pi, e^{-\pi^2\eta_2^2/4})$ function can be expanded in powers of $e^{-\pi^2\eta_2^2/4}$ as

$$\vartheta_3\left(n\,\pi, e^{-\pi^2\eta_2^2/4}\right) \approx \begin{cases} 1 + 2e^{-\pi^2\eta_2^2/4}, & \text{integer } n \\ 1 - 2e^{-\pi^2\eta_2^2/4}, & \text{half-integer } n. \end{cases} \tag{A11}$$

Expanding in powers of Δn and employing the above-mentioned approximations (A10) and (A11), the potential can be put in a parabolic form (15), where the spring constant k is given by

$$k = \frac{1}{2\,a^3\,b^2\,{\eta_1}^4} e^{-c/2} P\Big[2\,a\,b\,e^{-\frac{1}{2{\eta_1}^2}}\left((e^{2c}-1)^2\left(e^{\frac{\pi^2}{2c}}-2\right)d_y\,e^{\frac{1}{2{\eta_1}^2}}{\eta_1}^2 - 2\,a\,b\,e^{c/2}\,d_x\right) - \frac{1}{\pi\,\eta_2} e^{\frac{3c}{2}+\frac{3\pi^2}{4c}}$$
$$\times\left(-6\,e^c + 6\,e^{2c} + 2\,e^{3c} + e^{\frac{\pi^2}{4c}} - 3\,e^{c+\frac{\pi^2}{4c}} - 3\,e^{2c+\frac{\pi^2}{4c}} + e^{3c+\frac{\pi^2}{4c}} - 2\right)P\,\gamma\,\eta_1\Big], \tag{A12}$$

and the constant energy background is given by

$$V_0 = \frac{1}{8\,a^2\,b^2}\,P\Big[8\,a\,b\,e^{-\frac{5c}{2}-\frac{1}{2{\eta_1}^2}}\left(2\,a\,b\,e^{5c/2}\,d_x\left(e^{\frac{1}{2{\eta_1}^2}}-1\right) + \left(4\,e^{5c/2} + 6\,e^{4c} + 4\,e^{9c/2} - e^{\frac{\pi^2}{2c}} + 2\,e^{\frac{5c}{2}+\frac{\pi^2}{2c}} - 3\,e^{4c+\frac{\pi^2}{2c}} + 2\,e^{\frac{9c}{2}+\frac{\pi^2}{2c}}\right.\right.$$
$$\left.\left. + 2\right)d_y\,e^{\frac{1}{2{\eta_1}^2}}\right) - \frac{1}{\pi\,\eta_1\eta_2} 2\,e^{\frac{3\pi^2}{4c}}\left(-8\,e^c + 2\,e^{4c} + 3\,e^{\frac{\pi^2}{4c}} + 4\,e^{c+\frac{\pi^2}{4c}} + e^{4c+\frac{\pi^2}{4c}} + 6\right)\gamma\,P\Big], \tag{A13}$$

where $a = e^{\frac{2}{{\eta_2}^2}} + 1$, $b = e^{\frac{\pi^2{\eta_2}^2}{2}} + 2$, and $c = \frac{1}{{\eta_2}^2}$.

[1] D. N. Christodoulides and R. I. Joseph, Opt. Lett. **13**, 794 (1988).
[2] H. S. Eisenberg, Y. Silberberg, R. Morandotti, A. R. Boyd, and J. S. Aitchison, Phys. Rev. Lett. **81**, 3383 (1998).
[3] C. Mejia-Cortes, R. A. Vicencio, and B. A. Malomed, Phys. Rev. E **88**, 052901 (2013).
[4] A. B. Aceves, C. De Angelis, T. Peschel, R. Muschall, F. Lederer, S. Trillo, and S. Wabnitz, Phys. Rev. E **53**, 1172 (1996).
[5] R. Carretero-González, J. D. Talley, C. Chong, and B. A. Malomed, Physica D (Amsterdam) **216**, 77 (2006).
[6] I. E. Papacharalampous, P. G. Kevrekidis, B. A. Malomed, and D. J. Frantzeskakis, Phys. Rev. E **68**, 046604 (2003).
[7] Y. S. Kivshar and B. A. Malomed, Rev. Mod. Phys. **61**, 763 (1989).
[8] Y. S. Kivshar and D. K. Campbell, Phys. Rev. E **48**, 3077 (1993).
[9] L. Brizhik, A. Eremko, L. Cruzeiro-Hansson, and Y. Olkhovska, Phys. Rev. B **61**, 1129 (2000).
[10] P. G. Kevrekidis, I. G. Kevrekidis, A. R. Bishop, and E. S. Titi, Phys. Rev. E **65**, 046613 (2002).
[11] M. Johansson and P. Jason, in *Breather Mobility and the Peierls-Nabarro Potential: Brief Review and Recent Progress*, edited by J. F. R. Archilla, N. Jiménez, V. J. Sánchez-Morcillo, and L. M. García-Raffi, Quodons in Mica, Springer Series in Materials Science (Springer, New York, 2015).
[12] See J. Cuevas and B. A. Malomed, in Ref. [26].
[13] I. L. Garanovich, S. Longhi, A. A. Sukhorukov, and Y. S. Kivshar, Phys. Rep. **518**, 1 (2012).
[14] J. W. Fleischer, M. Segev, N. K. Efremidis, and D. N. Christodoulides, Nature (London) **422**, 147 (2003).
[15] R. Keil, M. Heinrich, F. Dreisow, T. Pertsch, A. Tünermann, S. Nolte, D. N. Christodoulides, and A. Szameit, Sci. Rep. **1**, 94 (2011).
[16] K. M. Aghdami, M. Golshani, and R. Kheradmand, IEEE Photonics J. **4**, 1147 (2012).
[17] D. N. Christodoulides and E. D. Eugenieva, Phys. Rev. Lett. **87**, 233901 (2001).
[18] P. G. Kevrekidis, K. O. Rasmussen, and A. R. Bishop, Phys. Rev. E **61**, 2006 (2000).
[19] U. A. Khawaja, P. S. Vinayagam, and S. M. Al-Marzoug, Phys. Rev. A **97**, 023820 (2018).
[20] L. Hadžievski, A. Maluckov, M. Stepić, and D. Kip, Phys. Rev. Lett. **93**, 033901 (2004).
[21] R. A. Vicencio and M. Johansson, Phys. Rev. E **73**, 046602 (2006).
[22] P. G. Kevrekidis, B. A. Malomed, A. Saxena, A. R. Bishop, and D. J. Frantzeskakis, Phys. Rev. E **91**, 043201 (2015).
[23] V. A. Brazhnyi and B. A. Malomed, Phys. Rev. E **83**, 016604 (2011).
[24] Z. Chen, J. Liu, S. Fu, Y. Li, and B. A. Malomed, Opt. Express **22**, 29679 (2014).
[25] A. Hause, H. Hartwig, M. Bohm, and F. Mitschke, Phys. Rev. A **78**, 063817 (2008).
[26] P. G. Kevrekidis, *The Discrete Nonlinear Schrödinger Equation Mathematical Analysis, Numerical Computations and Physical Perspectives* (Springer eBooks, New York, 2009).
[27] B. Malomed and M. I. Weinstein, Phys. Lett. A **220**, 91 (1996).
[28] B. A. Malomed, Prog. Opt. **43**, 71 (2002).
[29] Y. V. Kartashov, B. A. Malomed, and L. Torner, Rev. Mod. Phys. **83**, 247, (2011); **83**, 405(E) (2011).

[30] P. G Kevrekidis, K. Ø. Rasmussen, and A. R. Bishop, Int. J. Mod. Phys. B **15**, 2833 (2001).

[31] U. Peschel, R. Morandotti, J. M. Arnold, J. S. Aitchison, H. S. Eisenberg, Y. Silberberg, T. Pertsch, and F. Lederer, J. Opt. Soc. Am. B **19**, 2637 (2002).

[32] H. S. Eisenberg, R. Morandotti, Y. Silberberg, J. M. Arnold, G. Pennelli, and J. S. Aitchison, J. Opt. Soc. Am. B **19**, 2938 (2002).

[33] U. Al Khawaja, S. M. Al-Marzoug, and H. Bahlouli, Commun. Nonlinear Sci. Numer. Simul. **46**, 74 (2017).